


**Second-order mean-field approximation for calculating dynamics in Au-nanoparticle networks**Evan Wonisch<sup>1</sup>, Jonas Mensing, and Andreas Heuer<sup>1</sup>*Institute of Physical Chemistry, University of Münster, 48149 Münster, Germany* (Received 24 February 2024; accepted 1 August 2024; published 3 September 2024)

Exploiting physical processes for fast and energy-efficient computation bears great potential in the advancement of modern hardware components. This paper explores nonlinear charge tunneling in nanoparticle networks, controlled by external voltages. The dynamics are described by a master equation, which expresses the time-evolution of a distribution function over the set of charge occupation numbers. The driving force behind this evolution is charge tunneling events among nanoparticles and their associated rates. We introduce two mean-field approximations to this master equation. By parametrization of the distribution function using its first- and second-order statistical moments, and a subsequent projection of the dynamics onto the resulting moment manifold, one can deterministically calculate expected charges and currents. Unlike a kinetic Monte Carlo approach, which extracts samples from the distribution function, this mean-field approach avoids any random elements. A comparison of results between the mean-field approximation and an already available kinetic Monte Carlo simulation demonstrates great accuracy. Our analysis also reveals that transitioning from a first-order to a second-order approximation significantly enhances the accuracy. Furthermore, we demonstrate the applicability of our approach to time-dependent simulations, using Eulerian time-integration schemes.

DOI: [10.1103/PhysRevE.110.034103](https://doi.org/10.1103/PhysRevE.110.034103)**I. INTRODUCTION**

Disordered networks of Au nanoparticles [1], interconnected by organic molecules, exploit physical processes for computation. Each nanoparticle (NP), serving as a conductive island, is separated from its nearest neighbors by an insulating organic molecule. When electrons accumulate on a particular NP, they can tunnel through the insulator to an adjacent NP if the potential difference between both NPs exceeds the repelling force of the Coulomb energy [2,3]. This *Coulomb blockade* phenomenon equips each NP-to-NP junction with a nonlinear activation function, establishing a network of nonlinear functions analogous to a software-based artificial neural network (ANN). For an extensive experimental study on NP assemblies and their charge transport properties, refer to [4].

The network is surrounded by electrodes categorized as input, output, or control electrodes. Input and output electrodes correspond to the input and output layers of an ANN, while applying voltages to the control electrodes allows us to modify the internal landscape of NP potentials. Different potential landscapes, which affect the evaluation of those nonlinear functions, result in variable charge tunneling dynamics and, ultimately, in variable input-output relationships. Consequently, one can tune the set of applied control electrode voltages through genetic algorithms or backpropagation [1,5] and seek configurations in which the system can accomplish a given task.

The phase space of the system encompasses all possible charge occupation numbers within the network. Its charge tunneling dynamics are defined by the master equation, formulated as a set of differential rate equations [6,7]. The time evolution described by these equations can be solved

with a kinetic Monte Carlo (KMC) algorithm [3,6,8–10]. This approach efficiently reduces the infinite phase space to a physically meaningful subset, despite its intrinsic stochastic nature. Attempting to formulate an exact deterministic solution for the master equation, one faces exponential computational complexity arising from the size of phase space. Consequently, exact solutions are practically limited to very small systems. A strategy to formulate a deterministic solution with manageable polynomial complexity involves the application of mean-field approximation. The mean-field approximations simplify our network of NPs by replacing interactions to any NP with an average or effective interaction, significantly reducing the computational complexity. In this context, a first-order mean-field approximation for charge tunneling dynamics was introduced in [11]. These ideas have also been used to solve the master equation in socioeconomic population dynamics and migration processes [12–15]. In addition, similar concepts have also been used to describe triplet-triplet annihilation in the phosphorescent emission layers of light-emitting diodes [16].

In this work, we present a systematic approach that extends previous mean-field approximations to higher orders. We apply the mean-field approximation to the master equation describing single electronic tunneling dynamics. However, these concepts should also be applicable to any kind of stochastic processes where constituents hop between neighboring discrete sites. Specifically, we explore the second-order method, demonstrating its superior performance over the first-order method while maintaining high efficiency. An illustrative step towards analyzing time dependency and the investigation of nonlinear input-output electrode relationships is undertaken.

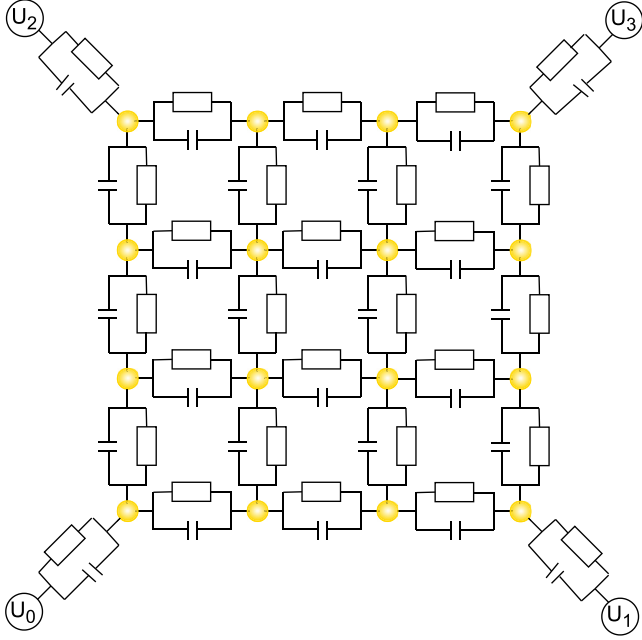


FIG. 1. A  $4 \times 4$  nanoparticle network with four electrodes  $U_0$ ,  $U_1$ ,  $U_2$ , and  $U_3$ . The electrodes are attached at the corners. The tunnel junctions are depicted as capacitors and resistors in parallel.

## II. THEORETICAL BACKGROUND

As we want to validate the mean-field algorithm in a controlled and simple environment, the network is modeled as a collection of  $N$  gold-NPs arranged in a grid lattice, some of which are connected to electrodes (see Fig. 1). We are aware that different network structures might give rise to more functionality. However, the focus in this paper is the testing of the algorithm. Please note that the mean-field approach, as defined and applied in this work, can be directly transformed to much more general cases.

The occupation number  $n \in \mathbb{Z}$  represents the number of excess electrons residing on a NP (island). This description will suffice to build the phase space  $\Omega$ . For  $N$  particles, the phase space is thus

$$\Omega = \mathbb{Z}^N. \quad (1)$$

The state of the system is described by a state vector  $\vec{n} \in \Omega$  which contains occupation numbers for excess electrons on each island. The network topology is encoded in a capacitance matrix, linking nearest neighbors by their mutual capacitance. The internal electrostatic energy can thus be calculated. Due to their proximity, electrons can tunnel through junctions between nearest neighbors. The tunnel rates will be described according to a zero-dimensional *orthodox tunnel theory* [17]. The tunnel rate  $\Gamma$  for an electron from one position to another depends on the difference in Helmholtz free energy  $\Delta F$  associated with this tunnel process,

$$\Gamma = -\frac{\Delta F}{e^2 R} \left[ 1 - \exp \frac{\Delta F}{k_B T} \right]^{-1}. \quad (2)$$

We restrict our model to single-electron tunneling. For a more complete description of single-electron tunneling

applied to nanoparticle networks, we refer the reader to Ref. [8] or [10].

It is important to mention that the free energy  $\Delta F$  governing the underlying transition rate not only depends on the population of the two involved islands, but also on the complete state vector  $\vec{n}$  due to the network of capacitors.

We introduce a distribution function  $\rho$  over phase space  $\Omega$  which assigns a probability  $\rho(\vec{n})$  to each possible system state  $\vec{n}$  [7,11]. The tunnel rates describe the tunneling of electrons between islands or electrodes and can be interpreted as the transition rate from states  $\vec{n}$  to  $\vec{m}$ , denoted as  $\Gamma_{\vec{n}\vec{m}}$ . Hence, the rate for an electron to tunnel from island  $i$  to island  $j$  is the transition rate from state  $\vec{n}$  to state  $\vec{n} - \vec{e}_i + \vec{e}_j$ , where the latter is missing one electron at index  $i$  and has an additional one at index  $j$ .  $\vec{e}_i$  is the  $i$ th basis vector in  $\Omega$ . If an electrode is connected to island  $i$ , two more transition rates are possible: For an electron tunneling towards the island, a transition from state  $\vec{n}$  to state  $\vec{n} + \vec{e}_i$ , the rate  $\Gamma_{\vec{n}\vec{n}+\vec{e}_i}$  is associated. For the reverse process, a minus sign must be taken. All other transition rates are zero.

The dynamics of the distribution function are governed by the following master equation:

$$\partial_t \rho(\vec{n}) = \sum_{\vec{m} \neq \vec{n}} [\Gamma_{\vec{m}\vec{n}} \rho(\vec{m}) - \Gamma_{\vec{n}\vec{m}} \rho(\vec{n})]. \quad (3)$$

The equilibrium distribution function is found when  $\partial_t \rho(\vec{n}) = 0 \forall \vec{n}$ . Afterward, expectation values of quantities of interest can be taken. From a nanoparticle, the electron can hop to another nanoparticle or to an attached electrode (or vice versa). This is captured by the following phase-space functions: The current flowing from particle  $i$  to particle  $j$ ,

$$I_{ij}(\vec{n}) = \Gamma_{\vec{n}\vec{n}+\vec{e}_j-\vec{e}_i} - \Gamma_{\vec{n}\vec{n}-\vec{e}_j+\vec{e}_i}; \quad (4)$$

the current flowing towards particle  $i$  from its attached electrode,

$$I_{ei}(\vec{n}) = \Gamma_{\vec{n}\vec{n}+\vec{e}_i} - \Gamma_{\vec{n}\vec{n}-\vec{e}_i}; \quad (5)$$

and the total current flowing to particle  $i$ ,

$$I_i(\vec{n}) = \sum_{j \neq i} I_{ji}(\vec{n}) + I_{ei}(\vec{n}). \quad (6)$$

Furthermore, phase-space functions with opposite sign are introduced, which are useful later,

$$I_{ij}^\dagger(\vec{n}) = \Gamma_{\vec{n}\vec{n}+\vec{e}_j-\vec{e}_i} + \Gamma_{\vec{n}\vec{n}-\vec{e}_j+\vec{e}_i}, \quad (7)$$

$$I_{ei}^\dagger(\vec{n}) = \Gamma_{\vec{n}\vec{n}+\vec{e}_i} + \Gamma_{\vec{n}\vec{n}-\vec{e}_i}, \quad (8)$$

$$I_i^\dagger(\vec{n}) = \sum_{j \neq i} I_{ji}^\dagger(\vec{n}) + I_{ei}^\dagger(\vec{n}). \quad (9)$$

For the subsequent equations, we use the convention that  $I_{ei} = 0$  if there is no direct connection between island  $i$  and an electrode.

Since storing and updating the entire distribution function is intractable for large systems, we will introduce efficient mean-field algorithms. For this purpose, equations of motion for the first and second moment are derived. With the

definition of the first moment,

$$\langle n_i \rangle = \sum_{\vec{n}} n_i \rho(\vec{n}), \quad (10)$$

its time evolution can be expressed as

$$\partial_t \langle n_i \rangle = \sum_{\vec{n}} n_i \partial_t \rho(\vec{n}). \quad (11)$$

Inserting Eq. (3) leads to

$$\partial_t \langle n_i \rangle = \sum_{\vec{n}} n_i \sum_{\vec{m} \neq \vec{n}} [\Gamma_{\vec{m}\vec{n}} \rho(\vec{m}) - \Gamma_{\vec{n}\vec{m}} \rho(\vec{n})]. \quad (12)$$

Expanding the sum to express the equation as an expectation value, one obtains

$$\partial_t \langle n_i \rangle = \sum_{\vec{v}} \rho(\vec{v}) \sum_{\vec{n} \neq \vec{v}} (n_i - v_i) \Gamma_{\vec{v}\vec{n}}. \quad (13)$$

Since the majority of transition rates  $\Gamma$  is zero because of *single-electron tunneling*, this expression simplifies to a very descriptive form. For a given  $\vec{v}$ ,  $\Gamma_{\vec{v}\vec{n}}$  is nonzero if  $\exists i, j$  with  $i \neq j$  and  $\vec{n} = \vec{v} \pm \vec{e}_i \mp \vec{e}_j$  for interparticle tunneling. If an electrode is attached to island  $i$ , two further transition rates, caused by the electrodes, can be nonzero:  $\Gamma_{\vec{v}\vec{v} \pm \vec{e}_i} \neq 0$ . Furthermore, all rates where  $n_i$  remains unchanged are not accounted for in the summation above since  $(n_i - v_i) = 0$  in that case. Equation (13) simplifies to

$$\partial_t \langle n_i \rangle = \sum_{j \neq i} \langle I_{ji} \rangle + \langle I_{ei} \rangle \quad (14)$$

$$= \langle I_i \rangle, \quad (15)$$

using Eqs. (4) and (5). This equation just reflects the conservation of electrons.

Analogously, the dynamics of higher-order moments are derived. For the second-order moments  $\langle n_i^2 \rangle$ , one can generalize Eq. (13) to

$$\partial_t \langle n_i^2 \rangle = \sum_{\vec{v}} \rho(\vec{v}) \sum_{\vec{n} \neq \vec{v}} (n_i^2 - v_i^2) \Gamma_{\vec{v}\vec{n}}. \quad (16)$$

Again, when taking care about the possible transitions, in analogy to the first-order method, one ends up, after a straightforward calculation, with

$$\partial_t \langle n_i^2 \rangle = \sum_{j \neq i} (2 \langle n_i I_{ji} \rangle + \langle I_{ji}^\dagger \rangle) + 2 \langle n_i I_{ei} \rangle + \langle I_{ei}^\dagger \rangle. \quad (17)$$

This can be abbreviated as

$$\partial_t \langle n_i^2 \rangle = \langle 2n_i I_i \rangle + \langle I_i^\dagger \rangle. \quad (18)$$

This procedure can be easily generalized to either mixed correlation terms such as  $\langle n_i n_j \rangle$  or higher-order moments. Due to the combination of simplicity and accuracy, observed after incorporation of the  $\langle n_i^2 \rangle$  correlation, in this work we restrict ourselves to the simplest extension beyond the first-order case.

Taking the term  $I_{ji}^\dagger$  as an example, one might be tempted to conclude that this term only depends on the populations of islands  $i$  and  $j$ . However, this is not true since the free energy  $\Delta F$ , governing the underlying transition rates, depends on the populations of all other NPs.

Note that all the equations so far are exact but intractable since the expectation values still require knowledge of the full exponentially complex distribution function. The mean-field approximation will be introduced in the next section, which allows one to express the expectation values just in terms of the first and (possibly) second moment.

### III. NUMERICAL METHODS

Strictly speaking, the calculation of, e.g.,  $\langle I_{ij} \rangle$  requires knowledge of the full distribution  $\rho(\vec{n}, t)$ , which requires the solution of the exact master equation (which we want to avoid). Let us assume that we need to evaluate an expectation value which explicitly depends on islands  $i$  and  $j$  such as  $\langle I_{ij} \rangle$ . Then we can proceed as follows:

*Mean-field approximation.* Following [11], we neglect all fluctuations of the electron occupation numbers  $n_k$  where the index  $k$  reflects all indices which fulfill  $k \neq i$  and  $k \neq j$ . The  $\{n_k\}$  are substituted by their average values  $\{\langle n_k \rangle\}$ . This is a natural choice because the transition rates from NP  $i$  to cluster  $j$  will naturally most strongly depend on the number of electrons on both clusters, whereas one may hope that the remaining clusters only act via their average electron occupation. Then the expectation value  $\langle I_{ij} \rangle$  just requires an average over the two-dimensional distribution  $\tilde{\rho}(n_i, n_j)$ .

*Factorization.* Furthermore, we neglect correlations among adjacent clusters. Preliminary KMC simulations have shown that these correlations are small. This step strongly simplifies the realization of the next step. Thus, we write  $\tilde{\rho}(n_i, n_j) = \tilde{\rho}_i(n_i) \cdot \tilde{\rho}_j(n_j)$ . To simplify the notation, we just abbreviate each factor as  $\tilde{\rho}(n)$  with  $n \in \{i, j\}$ . When an island is directly connected to an electrode, terms with just one index also occur. For these terms, no factorization is required.

*Choice of  $\tilde{\rho}(n)$  based on knowledge of the first moment [mean-field-1 (MF1)].* If only information about the first moment is available, a natural choice, introduced in [11], reads

$$\tilde{\rho}(n) = \begin{cases} d & \text{for } n = \lceil \langle n \rangle \rceil \\ 1 - d & \text{for } n = \lfloor \langle n \rangle \rfloor \\ 0 & \text{otherwise,} \end{cases} \quad (19)$$

with  $d = \langle n \rangle - \lfloor \langle n \rangle \rfloor$ . Notably, this distribution has a mean  $\langle n \rangle$  and only assigns probabilities to the two occupation numbers adjacent to its mean. Using those approximations, Eq. (15) becomes closed for  $N$  particles. The variance reads  $d - d^2$ . This is the smallest possible variance of the electron occupation number.

*Numerical determination of  $\tilde{\rho}(n)$  based on additional information about the second moment [mean-field-2 (MF2)].* Also incorporating information about the second moment allows for a more realistic approximation of  $\tilde{\rho}(n)$ . Here, two different approaches are presented. First, we define  $\tilde{\rho}(n)$  for all  $n \in [-20, 20]$  and guarantee that  $\tilde{\rho}(n)$  has the correct first and second moments. However, the choice is not unique. Therefore, we additionally formulate an optimization problem that the distribution  $\tilde{\rho}$  shall maximize the entropy

$S = - \sum_n \tilde{\rho}(n) \log \tilde{\rho}(n)$  under boundary conditions,

$$\begin{aligned} G_0 &= \sum_n \tilde{\rho}(n) - 1 = 0, \\ G_1 &= \sum_n n \tilde{\rho}(n) - \langle n \rangle = 0, \\ G_2 &= \sum_n n^2 \tilde{\rho}(n) - \langle n^2 \rangle = 0. \end{aligned} \quad (20)$$

The solution can be directly obtained with the use of Lagrange parameters, yielding the discrete Gaussian distribution,

$$\tilde{\rho}(n) = \frac{1}{Z} e^{-\frac{(n-\mu)^2}{2\sigma^2}} \quad \text{for } n \in \mathbb{Z}. \quad (21)$$

The Lagrange multipliers  $Z$ ,  $\mu$ , and  $\sigma$  are determined numerically so that all three boundary conditions (20) are fulfilled.

*Analytical determination of  $\tilde{\rho}(n)$  based on additional information about the second moment [quick mean-field-2 (QMF2)].* For two reasons, the implementation of MF2 is relatively slow. First, the distribution function has to be evaluated for a large phase space; second, a numerical determination of the Lagrange parameters is required. Here we suggest a method which remedies both problems. First, we restrict ourselves to a phase-space size of 4, i.e., we have to determine four probabilities  $p_1, \dots, p_4$ . Here the four indices reflect subsequent natural numbers such that the two lower ones ( $n_1, n_2$ ) are below or equal to the current estimate ( $n$ ) and the other two ( $n_3, n_4$ ) just above. Second, rather than maximizing the standard Shannon entropy, we maximize

$$\tilde{S} = 1 - \sum_{m=1}^4 p_m^2. \quad (22)$$

Together with the boundary conditions,

$$\sum_{m=1}^4 p_m = 1, \quad (23)$$

$$\sum_{m=1}^4 n_m p_m = \langle n \rangle, \quad (24)$$

$$\sum_{m=1}^4 n_m^2 p_m = \langle n^2 \rangle, \quad (25)$$

we obtain, after a straightforward calculation,

$$\begin{aligned} p_1 &= \frac{1}{4}d^2 - \frac{11}{20}d + \frac{1}{4}(\Delta n)^2 + \frac{3}{20}, \\ p_2 &= -\frac{1}{4}d^2 + \frac{3}{20}d - \frac{1}{4}(\Delta n)^2 + \frac{11}{20}, \\ p_3 &= -\frac{1}{4}d^2 + \frac{7}{20}d - \frac{1}{4}(\Delta n)^2 + \frac{9}{20}, \\ p_4 &= \frac{1}{4}d^2 + \frac{1}{20}d + \frac{1}{4}(\Delta n)^2 - \frac{3}{20}. \end{aligned} \quad (26)$$

Thereby,  $d = \langle n \rangle - \lfloor \langle n \rangle \rfloor$  and  $(\Delta n)^2$  is the current estimate of the variance. The distribution will be referred to as  $p^2$ -4 distribution.

This specific choice of  $\tilde{S}$  can be rationalized in two ways. First, if  $1 - p_n$  is not too large,  $\tilde{S}$  emerges from a Taylor expansion of the Shannon entropy. Second, in analogy to the Shannon entropy,  $\tilde{S}$  has the property that the maximum under the normalization condition  $\sum_m p_m = 1$  reads  $p_m = \text{const}$ . Indeed, we later show that the resulting distribution  $\tilde{\rho}(n)$

hardly differs from using the Shannon entropy. We are aware that Eq. (22) is identical to the nonextensive Tsallis entropy for  $q = 2$  [18,19]. However, as outlined above, our choice of entropy is of a pure mathematical nature of a locally defined variable, such as the number of excess electrons on a specific NP. Thus, there is no relation to the question about the extensiveness of the system.

One technical issue needs to be discussed in more detail. Formally, the  $p_i$  can turn out to be negative. This would invalidate the interpretation as probabilities. Here, we restrict this discussion to  $d \leq 1/2$ . The results for  $d > 1/2$  follow from symmetry arguments and the relevant results for  $d > 1/2$  are found in the Appendix A.

From the general solutions, one would obtain  $p_3 < 0$  if  $(\Delta n)^2 > V_+ \equiv \frac{9}{5} + \frac{7}{5}d - d^2$  and  $p_4 < 0$  if  $(\Delta n)^2 < V_- \equiv \frac{3}{5} - \frac{1}{5}d - d^2$ . One can easily convince oneself that upon increasing or decreasing  $(\Delta n)^2$  first,  $p_3$  or  $p_4$  become negative, respectively, whereas  $p_1$  and  $p_2$  are still positive.

Now a simple strategy can be formulated. In the case of  $(\Delta n)^2 > V_+$ , one chooses  $p_3 = 0$ . The remaining  $p_i$  are completely determined by the three boundary conditions. One obtains

$$p_1 = \frac{1}{3}[d^2 - 2d + (\Delta n)^2], \quad (27)$$

$$p_2 = \frac{1}{2}[-d^2 + d - (\Delta n)^2 + 2], \quad (28)$$

$$p_4 = \frac{1}{6}[d^2 + d + (\Delta n)^2]. \quad (29)$$

In the regime  $V_+ \leq (\Delta n)^2 < 2 + d - d^2$ , all  $p_m$  are positive. In practical terms, this means that the reduction to a four-dimensional phase space is consistent as long as the variance is smaller than 2 (in the worst case,  $d = 0$ ). As shown for the specific examples below, this is always fulfilled. Otherwise, it would be straightforward to generalize these ideas to, e.g., a six-dimensional phase space.

In the other limit  $(\Delta n)^2 < V_-$ , one should choose  $p_4 = 0$ . Again, from consideration of the three boundary conditions, one obtains

$$p_1 = \frac{1}{2}[d^2 - d + (\Delta n)^2], \quad (30)$$

$$p_2 = -d^2 - (\Delta n)^2 + 1, \quad (31)$$

$$p_3 = \frac{1}{2}[d^2 + d + (\Delta n)^2]. \quad (32)$$

All  $p_i$  are non-negative as long as  $(\Delta n)^2 \geq d - d^2$ . Since  $d - d^2$  is the minimum variance which may occur (see also the discussion of the MF1 algorithm), one can always find a well-defined distribution in the limit of low variances.

This procedure results in similar probabilities as the discrete Gaussian at minimal computational cost. A comparison is shown in Fig. 2. Indeed, using the  $p^2$ -4 distribution shows little deviations from the complete as well as from the restricted Gaussian distributions.

In summary, the dynamics are projected onto the moment manifold, which has a much lower dimensionality. The resulting dynamics of moments together with the respective mean-field distribution serve as an approximation to the true dynamics.

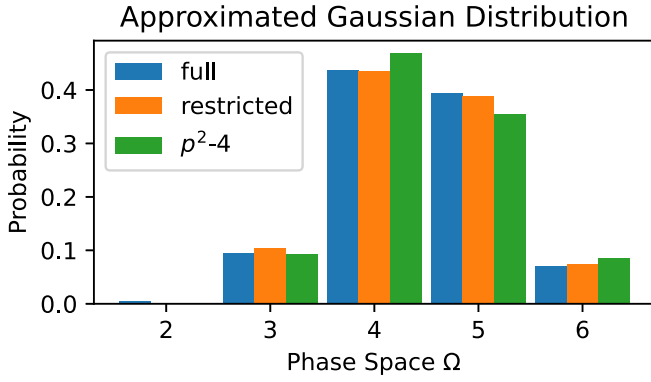


FIG. 2. Different approximations to the full Gaussian distribution with  $\langle n \rangle = 4.43$  and  $(\Delta n)^2 = 0.6$  are shown. Beyond the distributions used in MF2 and QMF2, we have also included the distribution resulting from maximization of the Shannon entropy, restricted to a four-dimensional phase space, denoted as restricted Gaussian distribution.

We mention in passing that the time evolution of the correlation of two adjacent NPs involves terms such as  $\langle n_i I_j \rangle$ . From the definition of  $I_j$ , it follows that three clusters are involved at the same time. Whereas for the QMF2 algorithm the tunneling rates have to be evaluated for 16 different cases  $(n_i, n_j)$ , an additional factor of 4 would emerge when taking into account the cross correlations.

To solve for the equilibrium configuration  $\partial_t \langle n_i \rangle = \partial_t \langle n_i^2 \rangle = 0$ , one can integrate the differential equations and obtain the full time-resolved dynamics. Since this is usually not required, more efficient algorithms finding the equilibrium point can be used. The ADAM algorithm [20], commonly used in machine learning to efficiently follow gradients of a cost function, can be applied and provides faster convergence and runtime performance by damping oscillations.

#### IV. SIMULATION RESULTS

Simulation results of first- and second-order methods are compared for systems of one or multiple nanoparticles. For one-particle systems, the exact distribution function can be obtained by solving the master equation as the reference. The abilities of MF1, MF2, and QMF2 will be assessed and compared. Since solving the master equation becomes computationally too complex for larger systems, a kinetic Monte Carlo method [8] (KMC) is used for generating samples of the distribution function, and thus reference data for larger systems. This method generates samples  $\vec{n}^{(j)} \in \Omega$  for  $j = 1, \dots, M$  of the distribution function  $\rho$ . The first- and second-order moments of the distribution can then be obtained by an estimate,

$$\langle n_i \rangle = \frac{1}{M} \sum_{j=1}^M n_i^{(j)}, \quad (33)$$

$$\langle n_i^2 \rangle = \frac{1}{M} \sum_{j=1}^M (n_i^{(j)})^2. \quad (34)$$

The currents involving electrodes are calculated by counting the number of jumps,  $\vec{n} \rightarrow \vec{n} \pm \vec{e}_i$ , for a given amount of time.

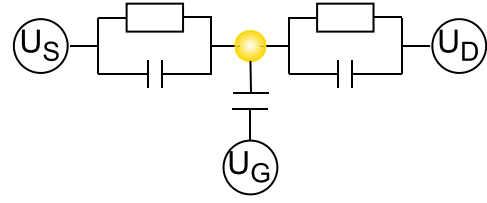


FIG. 3. A circuit diagram of the single-electron transistor. To the left and right, the two connected electrodes (source and drain) and the gate, realized by the capacitively coupled silicon substrate, are shown. Tunnel junctions are indicated as capacitors and resistors in parallel.

#### A. Single-electron transistor

The single-electron transistor is an important example of a network architecture consisting of just one nanoparticle. It is placed on a silicon substrate and connected to two electrodes who act as an input and output. Furthermore, a gate voltage can be applied to the silicon substrate, allowing for further manipulation of the potential landscape. A circuit diagram is shown in Fig. 3.

The calculated mean occupation number  $\langle n \rangle$  and its predicted standard deviation  $\Delta n$  are displayed in comparison to the correct master equation solution in Fig. 4. The first-order distribution [Eq. (19)] cannot account for high variances, which naturally appear in the master equation. The second-order method (MF2), using the full Gaussian distribution, does surpass this problem and accurately reproduces the mean and variance of the occupation number. The QMF2 method using the  $p^2-4$  distribution performs similarly to the MF2 method, thus providing a much closer approximate to the true distribution function and the ability to calculate more exact expectation values (such as the output current) or even evaluate the standard deviation of those.

#### B. Multiparticle systems

As a more relevant example, we consider square-shaped networks of nanoparticles of different sizes  $l \times l \times 1$  for  $2 \leq l \leq 10$ , exploring system sizes of up to one-hundred nanoparticles, which enter the range of experimentally realized systems. Four electrodes are attached to the corners of the network, providing a variety of input voltages, as well as a gate voltage. The systems are equilibrated and currents at electrode 3, being signified as the output-electrode, are calculated. An example of such a system is shown in Fig. 1. While the system size is varied from  $2 \times 2 \times 1$  up to  $10 \times 10 \times 1$ , the electrode positions stay at the corners. As the MF2 method is numerically quite expensive for large systems, the focus lies on the QMF2 method.

Obtaining the equilibrium occupation numbers for the KMC, MF1, and QMF2 algorithms and plotting them in their spatial configuration (here for a  $10 \times 10$  system) results in Fig. 5.

##### 1. Accuracy comparison

The main improvement of the second-order method lies in the estimation of electrode currents, which are the main

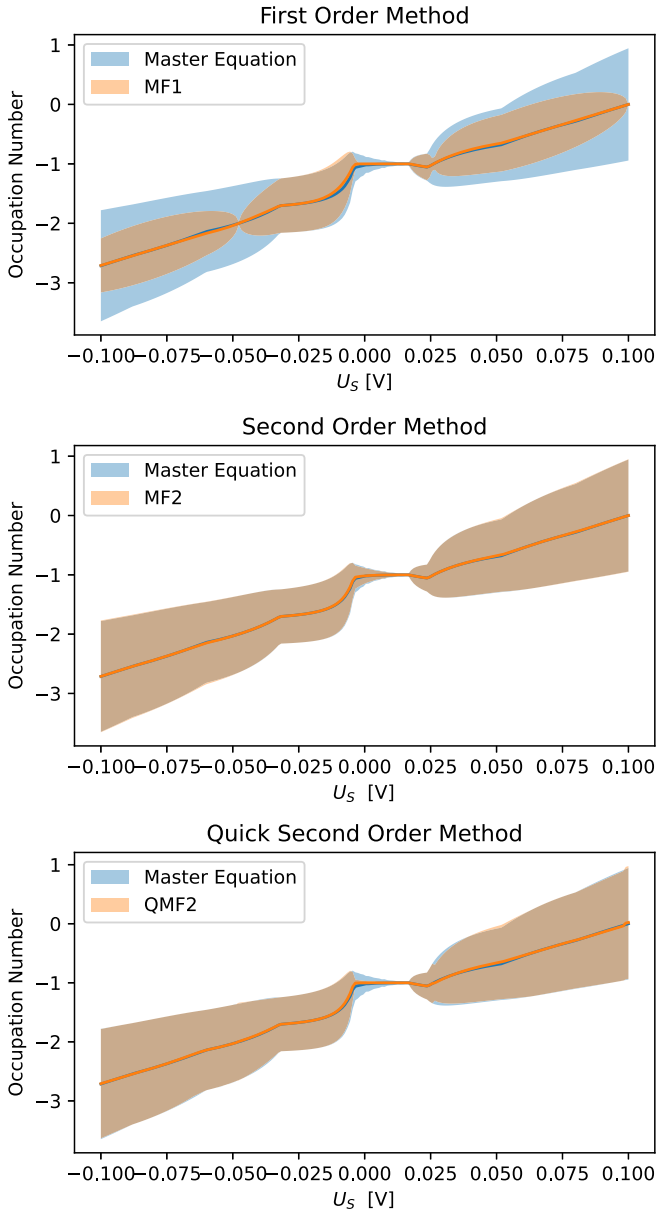


FIG. 4. For a nonzero gate voltage of 0.05 V, the first-order method has problems replicating the mean occupation number and its variance. The second-order methods still accurately reproduce the mean and variance of the master equation. The shaded areas represent the interval of  $\pm\Delta n$  predicted by the methods compared to the master equation. It can be seen that for low input voltages, no charge resides on the island, a nonlinear effect called the Coulomb blockade (see [8]).

point of interest when mapping functionalities to input-output electrode dependencies. Compared to the KMC reference data, whose currents are sampled up to numerical precision of 0.5%, requiring an average amount of  $74 \times 10^6$  samples, the first-order method estimates the currents with a relative error of  $(10.47 \pm 0.5)\%$  on average over all system sizes, which is outperformed by the second-order method with an error of  $(3.25 \pm 0.5)\%$ , shown in Table I. As the estimation of mean occupation numbers behaves similarly in MF1 and QMF2, the improved output current estimation

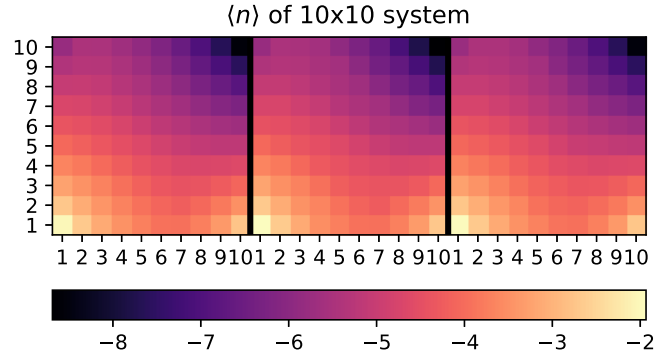


FIG. 5. For a random voltage configuration, the mean occupation numbers are plotted, from left to right, for the KMC, first-order MF1, and second-order QMF2 method. Its spatial variation is reflected by the colour-code. Results of all methods lie in qualitative agreement.  $E_1 = -0.10$  V,  $E_2 = -0.23$  V,  $E_3 = 0.07$  V,  $E_4 = 0.05$  V are set and the gate voltage is  $G = 0.13$  V.

arises through the additional incorporation of the second moment.

### 2. Predicted means and variances

To evaluate the response to adiabatically changed voltage configurations, 200 continuously varied voltage configurations, shown in Fig. 6, are applied to a  $4 \times 4$  system, as used above. The predicted quantities  $\langle n_i \rangle$ ,  $\langle n_i^2 \rangle$  and their deviations in different algorithms are depicted as the system is equilibrated for each voltage configuration. See Fig. 7 for the island connected to electrode  $U_0$ . Naturally, the second-order method QMF2 more closely matches the variances. However, importantly, for some configurations (e.g., around 130–140), the first moment is also predicted much better, although for this specific island in this regime the variance is close to its minimum value, i.e., seeing similar results for MF1 and QMF2. This exemplifies the superiority of QMF2, even if one is only interested in the first moments.

### C. Time-dependent systems

The algorithms at hand not only allow for equilibrium-state analysis, but can be easily used to calculate the system's response to time-dependent voltage configurations. A Fourier analysis is conducted to quantify different types of

TABLE I. Relative errors in output current ( $\pm 0.5\%$ ).

System size	MF1 (%)	QMF2 (%)
4	6.72	2.89
9	7.81	2.29
16	9.20	2.50
25	10.53	3.02
36	11.66	3.44
49	12.04	3.29
64	12.39	4.14
81	12.40	4.62
100	11.50	5.52

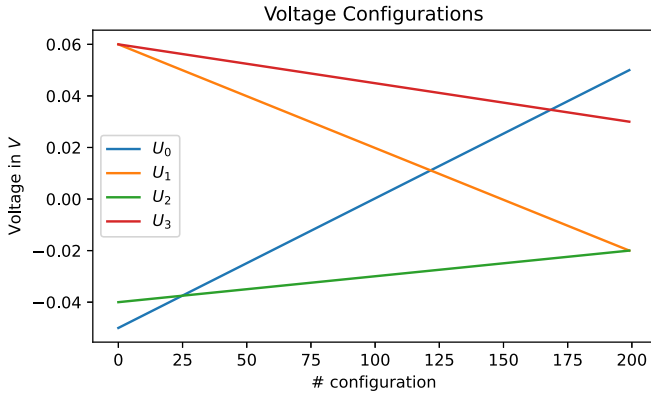


FIG. 6. 200 voltage configurations for the four electrodes ( $U_0$  to  $U_3$ ) are taken continuously to show the response of the system.

nonlinearities characteristic to the system. The system in question is a  $3 \times 3$  system (analogous to the systems above) with two input electrodes attached at the diagonals. Output electrodes are attached to the remaining corners with a voltage set to zero. Two cosine voltages are applied with amplitude  $U_0 = 0.1$  V and different frequencies,  $\omega_1 = 2$  GHz and  $\omega_2 = 7$  GHz. A nonlinear frequency mixture is observed when the

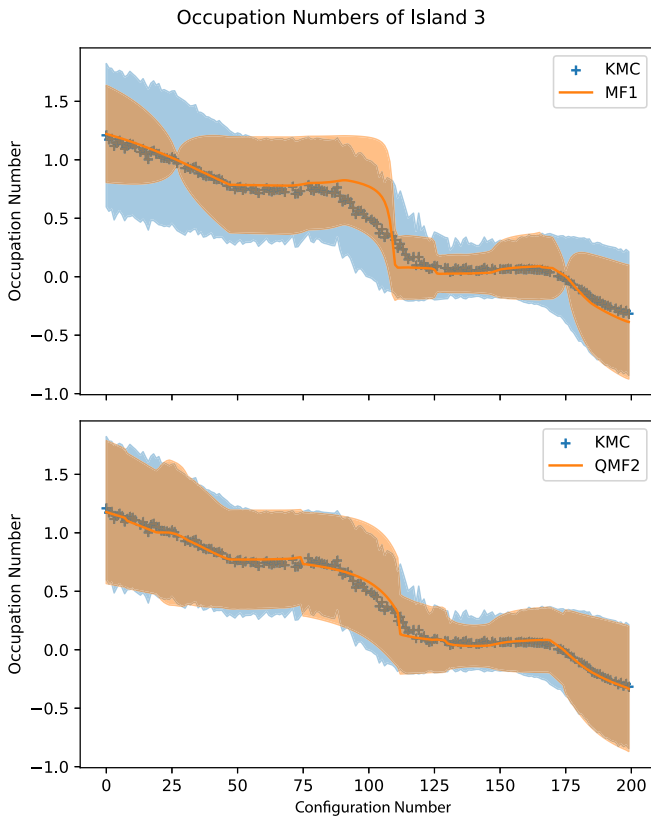


FIG. 7. The mean and the interval of  $\pm \Delta n$  resulting from the first- and second-order methods are shown for the island connected to electrode  $U_0$ . The KMC means are highlighted as red crosses, and the red shaded area corresponds to their standard deviation. It can be seen that the second-order method achieves a better approximation than the first-order method, thus allowing for more precise estimation of the expectation values.

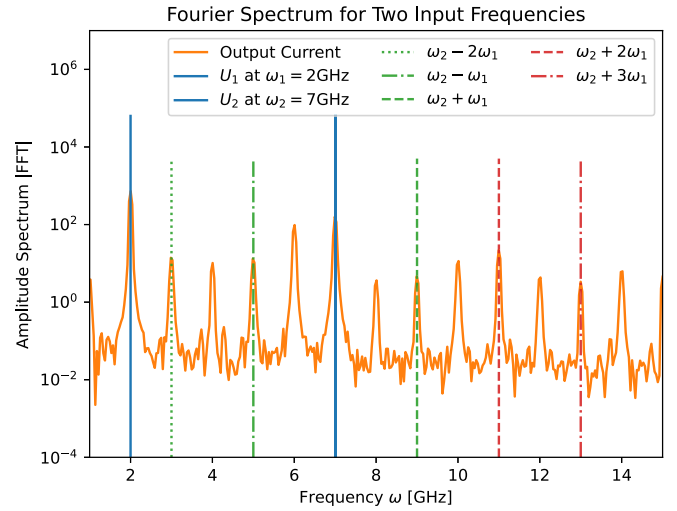


FIG. 8. Subjecting the system to two different input signals at different electrodes (diagonals), the output current not only includes their frequencies but also a nonlinear response consisting of linear combinations of those frequencies.

system is subjected to the two different oscillating input voltages. The inputs couple and produce linear combinations of their frequencies in the output spectrum, showing that the system is, in practice, capable of multiplying two signals at different electrodes; see Fig. 8. This behavior corresponds to an AND logic gate. Further tuning of control voltages could result in more complex nonlinear behavior (e.g., calculating exponentials, acting as Boolean logic gates, or performing high-dimensional input-output transformations).

## V. CONCLUSION

To and enable an appropriate analysis of the system's properties to ultimately exploit the inherent physical phenomena for computation, the system's dynamics have to be simulated. A corresponding master equation governs the dynamics as a probability flow in the discrete phase space. This is infeasible to solve directly because the dimensionality of the phase space grows exponentially with the number of particles. Considering just two possible occupation numbers 0 and 1 for 100 islands would already exceed the capabilities as  $2^{100}$  configurations result. Beyond the standard KMC approach, we aimed to find methods to explore the dynamics deterministically. Conceptually, this is analogous to expressing the solution of a Langevin equation via a Fokker-Planck equation. For this purpose, guided by [11], we have derived equations governing the dynamics of the distribution's moments. Finding appropriate mean-field distributions by maximization of entropy and substituting the true distribution led to a class of mean-field algorithms. Its first- and second-order methods were presented. The incorporation of higher-order moments or information about covariances could further improve the accuracy, albeit with the disadvantage of longer simulation times. Already when transitioning from first to second order, a great improvement of accuracy is observed, enabling sufficient analysis of the system's properties.

We remind the reader that the Coulomb blockade of each nanoparticle is essential as it makes the system a concatenation of nonlinear switches which create its ability to map from inputs to outputs nonlinearly with rich and reconfigurable dynamics. These effects can easily be reproduced with the presented algorithms. Furthermore, input-output relationships can be computed, be it adiabatic or time dependent. Time-dependent investigations, which by simple Eulerian integration are easily obtained, were performed to show that the system nonlinearly couples the inputs of different electrodes, which is a prerequisite of evolving versatile functionalities.

Further investigations are needed to understand the effects of covariance between occupation numbers, which in the aforementioned algorithms was neglected. A further increase in accuracy could be expected at the cost of a longer runtime. The covariances could be key to understanding the systems' behavior for very low input voltages, for which all current algorithms have difficulty. Also, a C++ accelerated implementation would allow for quicker and more effective research. Using frameworks such as TENSORFLOW or JAX, an autodifferentiable implementation of the algorithm could be created to allow for identification of appropriate voltage configurations for difficult tasks, as backpropagation could be used and genetic algorithms become inefficient in high-dimensional spaces. It could be attempted to evolve the

system into classifiers or perform regression problems, as it is commonly done to benchmark algorithms and network architectures in Deep Learning. The flexibility of the system to change its input-output relationship could thus be assessed.

### ACKNOWLEDGMENTS

This work was funded by the Deutsche Forschungsgemeinschaft (DFG, German Research Foundation) through Project No. 433682494–SFB 1459. We would like to thank P. Bobbert and W.G. van der Wiel for helpful discussions.

### APPENDIX: $p^2$ -4 DISTRIBUTION

For  $p_1 = 0$ , the other probabilities amount to

$$p_2 = \frac{1}{2}d^2 - \frac{3}{2}d + \frac{1}{2}(\Delta n)^2 + 1, \quad (\text{A1})$$

$$p_3 = -d^2 + 2d - (\Delta n)^2, \quad (\text{A2})$$

$$p_4 = \frac{1}{2}d^2 - \frac{1}{2}d + \frac{1}{2}(\Delta n)^2. \quad (\text{A3})$$

Setting  $p_2 = 0$ , the other probabilities amount to

$$p_1 = \frac{1}{6}[d^2 - 3d + (\Delta n)^2 + 2], \quad (\text{A4})$$

$$p_3 = \frac{1}{2}[-d^2 + d - (\Delta n)^2 + 2], \quad (\text{A5})$$

$$p_4 = \frac{1}{3}[d^2 + (\Delta n)^2 - 1]. \quad (\text{A6})$$

- 
- [1] S. Bose, C. P. Lawrence, Z. Liu, K. Makarenko, R. M. van Damme, H. J. Broersma, and W. G. van der Wiel, Evolution of a designless nanoparticle network into reconfigurable Boolean logic, *Nat. Nanotechnol.* **10**, 1048 (2015).
- [2] W. G. Van der Wiel, S. De Franceschi, J. M. Elzerman, T. Fujisawa, S. Tarucha, and L. P. Kouwenhoven, Electron transport through double quantum dots, *Rev. Mod. Phys.* **75**, 1 (2002).
- [3] C. Wasshuber, Single-electronics-how it works. How it's used. How it's simulated, in *Proceedings of the International Symposium on Quality Electronic Design* (IEEE, Piscataway, NJ, 2002), pp. 502–507.
- [4] A. Zabet-Khosousi and A.-A. Dhirani, Charge transport in nanoparticle assemblies, *Chem. Rev.* **108**, 4072 (2008).
- [5] S. K. Esser, R. Appuswamy, P. Merolla, J. V. Arthur, and D. S. Modha, Backpropagation for energy-efficient neuromorphic computing, in *Advances in Neural Information Processing Systems*, edited by C. Cortes, N. Lawrence, D. Lee, M. Sugiyama, and R. Garnett (Curran Associates, Red Hook, New York, 2015), Vol. 28.
- [6] L. Fonseca, A. Korotkov, K. Likharev, and A. Odintsov, A numerical study of the dynamics and statistics of single electron systems, *J. Appl. Phys.* **78**, 3238 (1995).
- [7] F. Willy and Y. Darma, Modeling and simulation of single electron transistor with master equation approach, *J. Phys.: Conf. Ser.* **739**, 012048 (2016).
- [8] J. Mensing, W. G. van der Wiel, and A. Heuer, A kinetic Monte Carlo approach for Boolean logic functionality in gold nanoparticle networks, *Front. Nanotechnol.* **6**, 1364985 (2024).
- [9] C. Wasshuber, H. Kosina, and S. Selberherr, Simon-a simulator for single-electron tunnel devices and circuits, *IEEE Trans. Comput. Aided Des. Integr. Circuits Syst.* **16**, 937 (1997).
- [10] M. Šuvakov and B. Tadić, Modeling collective charge transport in nanoparticle assemblies, *J. Phys.: Condens. Matter* **22**, 163201 (2010).
- [11] C. P. Lawrence, *Evolving Networks To Have Intelligence Realized At Nanoscale*, Ph.D. thesis (University of Twente, Netherlands, 2018).
- [12] G. Haag, *Modelling with the Master Equation: Solution Methods and Applications in Social and Natural Sciences* (Springer, Cham, 2017).
- [13] G. Haag and W. Weidlich, A stochastic theory of interregional migration, *Geogr. Anal.* **16**, 331 (1984).
- [14] W. Weidlich, Stochastic migration theory and migratory phase transitions, *J. Non-Equilib. Thermodyn.* **11**, 261 (1986).
- [15] G. Haag and D. S. Dendrinios, Toward a stochastic dynamical theory of location: A nonlinear migration process, *Geogr. Anal.* **15**, 269 (1983).
- [16] M. Taherpour, C. van Hoesel, R. Coehoorn, and P. A. Bobbert, Accurate and fast master equation modeling of triplet-triplet annihilation in organic phosphorescent emission layers including correlations, *Phys. Rev. B* **105**, 085202 (2022).
- [17] D. Averin and K. Likharev, Single electronics: A correlated transfer of single electrons and Cooper pairs in systems of small tunnel junctions, in *Mesoscopic Phenomena in Solids, Modern Problems in Condensed Matter Sciences*, edited by B. Altshuler, P. Lee, and R. Webb (Elsevier, Amsterdam, 1991), Chap. 6, Vol. 30, pp. 173–271.
- [18] C. Tsallis, Possible generalization of Boltzmann-Gibbs statistics, *J. Stat. Phys.* **52**, 479 (1988).
- [19] G. Alomani and M. Kayid, Further properties of Tsallis entropy and its application, *Entropy* **25**, 199 (2023).
- [20] D. P. Kingma and J. Ba, ADAM: A method for stochastic optimization, [arXiv:1412.6980](https://arxiv.org/abs/1412.6980).